Observation of two ferromagnetic phases in Fe_3Mo_3N

T. Waki,[1,*] S. Terazawa,[1,†] Y. Tabata,[1] K. Sato,[2,‡] A. Kondo,[2] K. Kindo,[2] and H. Nakamura[1]
[1]*Department of Materials Science and Engineering, Kyoto University, Kyoto 606-8501, Japan*
[2]*The Institute for Solid State Physics, The University of Tokyo, Kashiwa 277-8581, Japan*
(Received 13 March 2014; revised manuscript received 18 June 2014; published 15 July 2014)

We report alloying-induced and field-induced ferromagnetism in the η-carbide-type compound Fe_3Mo_3N, which shows a non-Fermi-liquid behavior in the vicinity of a ferromagnetic quantum critical point. Co substitution induces ferromagnetism in $(Fe_{1-x}Co_x)_3Mo_3N$ in the composition range $0.05 \leqslant x \leqslant 0.60$. With increasing x, the magnetism varies from the Curie-Weiss-type paramagnetism with a maximum in the temperature dependence of the magnetic susceptibility to another paramagnetism without the maximum via a weak ferromagnetism. An itinerant electron metamagnetic transition is observed for low x at a magnetic field of ~14 T. The magnetic phase diagram, in which the alloying-induced and the field-induced ferromagnetic phases are separated, is different from conventional phase diagrams for weak ferromagnets. Taking account of the fact that a magnetic field induces a Fermi-liquid behavior, the quantum criticality for pure Fe_3Mo_3N appears to be dominated by the dispersive spin fluctuations observed in the alloying-induced ferromagnetic phase.

DOI: 10.1103/PhysRevB.90.014416 PACS number(s): 75.30.Kz, 75.50.Cc

I. INTRODUCTION

The quantum phase transition (QPT), which is induced by quantum fluctuations between ordered and disordered phases at zero temperature, is of interest. Weak itinerant electron magnets are appropriate for exploring QPT because magnetic order can easily be tuned by applying pressure or alloying. The self-consistent renormalization theory of spin fluctuation adequately describes the QPT, and hence non-Fermi-liquid (NFL) behaviors are expected in a quantum critical regime [1]. In some weak antiferromagnetic heavy-fermion compounds [2] and iron pnictides [3], not only NFL behaviors but also unconventional superconductivity have been found at around a quantum critical point (QCP).

QPT has been studied in weak itinerant electron ferromagnets (WIEFs) such as UGe_2 [4], MnSi [5], $ZrZn_2$ [6], and Ni_xPd_{1-x} [7]. Interestingly, the second-order ferromagnetic transition changes to first-order and the critical line bifurcates at the tricritical point before the system reaches a QCP. When the system intersects the bifurcated planes, a first-order itinerant electron metamagnetic transition (IEMT) is observed. These features in the phase diagram have commonly been observed in WIEF [8,9]. The first-order phase boundary of the IEMT is terminated at a critical end point (CEP), at which the transition is of second order. Instead of the QCP, the WIEF has a quantum critical end point (QCEP), a zero-temperature CEP in a finite magnetic field. At around the QCEP, anomalous quantum criticality is expected, and it has actually been found in $Sr_3Ru_2O_7$ [10], UGe_2 [11], UCoAl [12], etc.

Recently, we have observed NFL behaviors in a 3D ferromagnetic quantum critical regime [1,13,14]; in particular, we observed $-\log T$ divergence of specific heat divided by T and $T^{5/3}$ dependence of resistivity at low temperatures in the η-carbide-type compound Fe_3Mo_3N without tuning such as application of pressure and substitution [15]. In accordance with this fact, ferromagnetism is induced by Co substitution as reported by Prior and Battle [16]. In contrast to their report, we observed continuous variation in the magnetism of $(Fe_{1-x}Co_x)_3Mo_3N$, and we further report alloying-induced ferromagnetic order in the composition range $0.05 \leqslant x \leqslant 0.60$ that corresponds to a domelike ferromagnetic region surrounded by a paramagnetic phase in the magnetic phase diagram [17].

The magnetic susceptibility χ of Fe_3Mo_3N shows a Curie-Weiss (CW) temperature dependence at high temperature, and the curve exhibits a broad hump at around 75 K without the onset of magnetic order. The χ-T maximum behavior for the WIEF is known to be relevant to the IEMT [18–20]. As expected, we observed an IEMT in Fe_3Mo_3N at around 14 T [17].

In the light of the above discussion, we note that our system is in the vicinity of two kinds of ferromagnetic states. To examine the relationship between the observed NFL behaviors and alloying-induced and field-induced ferromagnetic phases, we performed a comprehensive study of the magnetism in $(Fe_{1-x}Co_x)_3Mo_3N$ and constructed an x-H-T phase diagram. Our study revealed that the field-induced ferromagnetic (FIF) phase is separate from the alloying-induced ferromagnetic (AIF) phase, and the resulting phase diagram is different from that proposed for WIEFs.

II. EXPERIMENTS

Polycrystalline samples of $(Fe_{1-x}Co_x)_3Mo_3N$ with $0 \leqslant x \leqslant 1$ were successfully synthesized by reducing and nitriding transition metal oxides [16,21]. Fe_2O_3, Co_3O_4, and MoO_3 were mixed in a molar ratio of $(1-x)/2{:}x/3{:}1$ and placed in a silica tube, and subsequently the mixture was fired in a gas stream of N_2 containing 10% H_2 at 700 °C for 48 h followed by heat treatment at 1000 °C for 48 h with intermediate grinding at least four times. The obtained samples were examined using x-ray diffraction and revealed to be in single phases. The lattice constant at room temperature decreases with increasing

*waki.takeshi.5c@kyoto-u.ac.jp
†Present address: Hitachi Metals, Ltd., 2-15-17 Egawa, Shimamoto-cho, Mishima-gun, Osaka 618-0013, Japan.
‡Present address: Ibaraki National College of Technology, Department of Natural Science, 886 Nakane, Hitachinaka 312-8508, Japan.

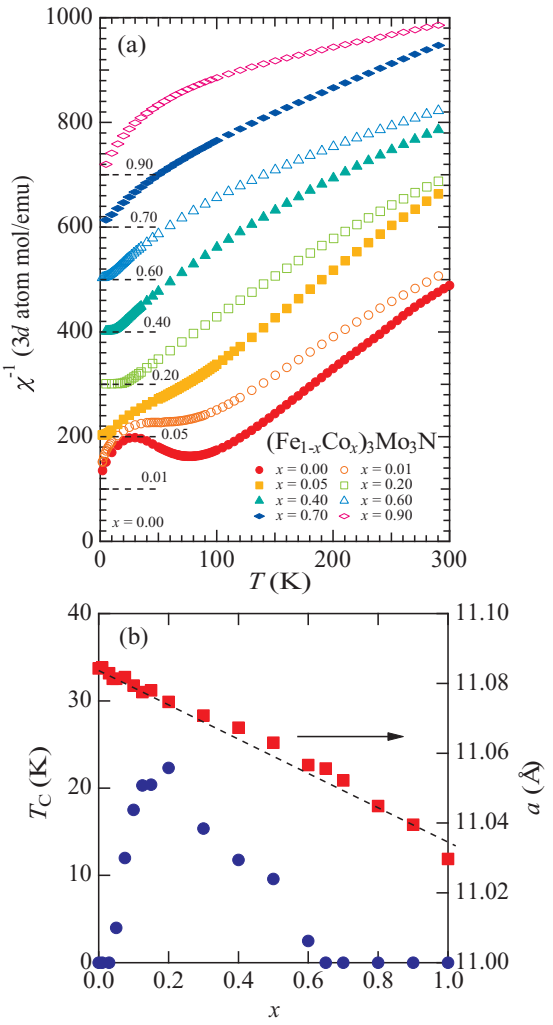

FIG. 1. (Color online) (a) Reciprocal susceptibility of $(Fe_{1-x}Co_x)_3Mo_3N$ for selected compositions. The data are offset and dashed lines represent their origins. (b) x dependence of T_C and lattice constant. The dashed line serves as a visual guide.

x values in accordance with Vegard's law, as shown in Fig. 1(b). Although Prior and Battle have reported a discontinuous T_C versus x curve because of the site preference of Co ions to the 32e site [16], the magnetism of our alloyed samples changes continuously with increasing x, as discussed below. We observed that the magnetism changes depending on the times of heat treatment; magnetic susceptibility after the first stage of heat treatment at 1000 °C is almost temperature independent at high temperatures showing a Pauli paramagnetic behavior, while it converges to a CW-type behavior after several heat treatments. The magnetization M at low fields was measured in the range from 1.8 to 300 K and up to 7 T using a SQUID magnetometer MPMS (Quantum Design) installed in the LTM center, Kyoto University. The temperature dependence of the magnetic susceptibility was measured under a field of 0.1 T with increasing temperature after the system was field cooled. The high-field magnetization up to 54 T was measured for $(Fe_{1-x}Co_x)_3Mo_3N$ using a pulse magnet installed in the ISSP, The University of Tokyo, over the temperature range of 1.3–100 K. Polycrystalline powder was filled into a cylindrical polyethylene tube that measured typically 6 mm in length and 2.5 mm in diameter. The value of magnetization was obtained by integrating the dM/dH signal induced in a pickup coil. The absolute value of M was corrected by using the magnetization data obtained using a SQUID magnetometer for fields up to 7 T.

III. RESULTS

A. Alloying-induced ferromagnetism

Figure 1 shows the reciprocal susceptibility χ^{-1} of $(Fe_{1-x}Co_x)_3Mo_3N$ for various compositions. At high temperatures a CW-type behavior was observed over the whole compositional range. As reported in a previous paper [17], χ at high temperatures can be fitted with a modified CW function

$$\chi = \frac{N_0(p_{\rm eff}\mu_B)^2}{3k_B(T-\theta)} + \chi_0, \quad (1)$$

where N_0 denotes the number of magnetic atoms per unit, $p_{\rm eff}$ the effective moment, μ_B the Bohr magneton, k_B the Boltzmann constant, θ the Weiss temperature, and χ_0 a temperature-independent term. The fitting was performed between $T = 150$ and 300 K for each x. The observed values of the various relevant parameters are listed in Table I. Corresponding to the χ-T maximum, a minimum of χ^{-1} is observed at 75 K in Fe_3Mo_3N. With increasing x, the observed anomaly or kink in the curve slightly shifts to lower temperatures and disappears at $x \simeq 0.10$. The linear extrapolation of χ^{-1} at low temperature for the composition range $0.05 \leqslant x \leqslant 0.60$ reaches zero at finite temperatures, thereby suggesting ferromagnetic interaction. Thermal hysteresis of the ferromagnetic

TABLE I. Magnetic parameters ($p_{\rm eff}$, θ, and χ_0) of $(Fe_{1-x}Co_x)_3Mo_3N$ deduced from the modified CW fitting. The values of p_s were obtained from the corresponding Arrott plot at 1.8 K. Curie temperature T_C and lattice constant a at room temperature are also listed.

x	$p_{\rm eff}(\mu_B$/ 3d atom)	θ (K)	$\chi_0(10^{-4}$ emu/ mol-f.u.)	T_C (K)	$p_s(\mu_B$/ 3d atom)	a (Å)
0.00	2.18	4.3	0			11.0843
0.01	2.35	−2.8	2.257			11.0846
0.03	2.17	13.2	2.277			11.0829
0.04	2.09	19.3	2.795			11.0813
0.05	2.12	22.6	0	4.0	0.0438	11.0813
0.075	1.99	30.2	5.358	12.0	0.116	11.0818
0.10	2.16	24.1	0	17.5	0.176	11.0794
0.125	2.12	24.0	0	20.3	0.196	11.0775
0.15	2.14	25.2	2.764	20.5	0.215	11.0780
0.20	2.15	22.0	3.823	22.3	0.222	11.0747
0.30	2.07	14.1	6.665	15.4	0.185	11.0708
0.40	1.95	10.4	8.984	11.8	0.155	11.0673
0.50	1.92	8.2	8.901	9.5	0.143	11.0630
0.60	2.00	0	14.13	2.5	0.062	11.0566
0.65	1.99	−7.6	10.11			11.0556
0.70	2.16	−16.0	10.18			11.0522
0.80	2.27	−28.1	8.546			11.0449
0.90	2.05	−53.5	19.97			11.0392
1.00	1.99	−70.4	42.80			11.0297

transition was observed only for $x = 0.05$. In the experimental resolution, no hysteresis was observed for $0.075 \leqslant x \leqslant 0.60$, suggesting that the ferromagnetic transition is of second order. For $x \geqslant 0.65$, χ^{-1} decreases monotonically with decreasing temperature, showing a CW-type behavior without onset of ferromagnetic order.

Figure 1(b) shows the plot of x versus T_C estimated from the Arrott plot (as described below), together with lattice constants at room temperature. When Fe is substituted by Co, ferromagnetism appears at $x \simeq 0.05$. T_C increases rapidly to reach a maximum (22.3 K) at $x = 0.20$. Subsequently, it decreases with a more moderate slope of $|dT_C/dx|$ than that at $0.05 \leqslant x \leqslant 0.20$ and becomes zero at $x \simeq 0.60$, resulting in a phase diagram with a domelike ferromagnetic region.

Figure 2 shows the Arrott plots at low fields and at $T = 1.8$ K for Co-doping-induced ferromagnetic and nearly ferromagnetic metals. We can observe a high degree of linearity for high Co concentrations including paramagnetic samples with the slope being nearly x independent. The Arrott plots for $x = 0.05$–0.15 deviate progressively upward due to the presence of the paramagnetic component that undergoes an IEMT at a higher field (see below). The spontaneous moment

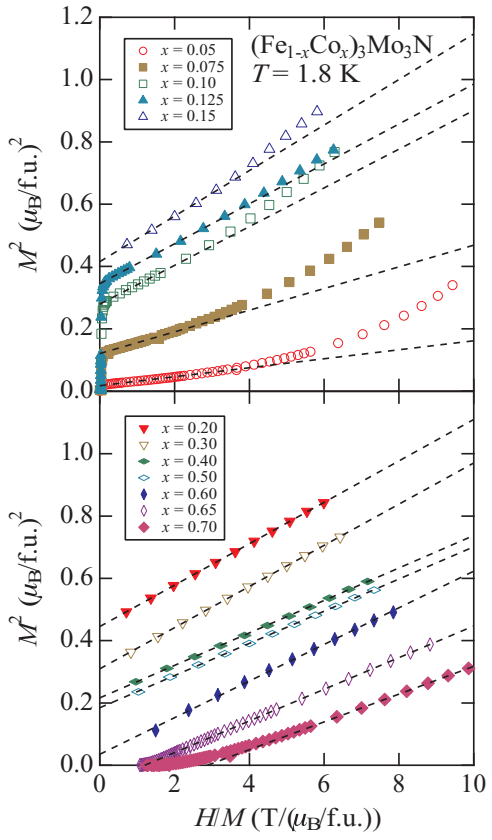

FIG. 2. (Color online) Arrott plots corresponding to the low-field region for the composition range of $0.05 \leqslant x \leqslant 0.70$. Dashed lines indicate the best linear fitting at low fields. For $0.20 \leqslant x \leqslant 0.70$, the Arrott plots are linear over wide field regions. For $0.05 \leqslant x \leqslant 0.15$, the Arrott plots are linear only at low fields but deviate progressively upwards at high fields; this phenomenon is often observed in the paramagnetic state far above T_C, suggesting the coexistence of the doping-induced ferromagnetic and the paramagnetic fluctuations.

p_s is estimated by extrapolating linearly M^2 to $H/M = 0$. Positive values of p_s, corresponding to the AIF phase, are obtained in the range of $0.05 \leqslant x \leqslant 0.60$.

In general, the existence of large density of states (DOS) immediately above the Fermi energy is predictable with the rigid band model. The domelike ferromagnetic region of our system can be explained as follows. With increasing Co concentration, lower levels in DOS are initially occupied by electrons to gain exchange energy, resulting in band polarization. When the Fermi level reaches the DOS maximum, T_C reaches a maximum at $x = 0.20$. With further increase in electrons, the band begins to be filled, and the magnetism becomes weaker. The attenuation of the magnetism beyond $x = 0.20$ may also be explained in terms of the volume-induced change in the band width; the smaller the volume, the less enhanced is the magnetism.

B. Field-induced ferromagnetism

From the *pulsed* high-field magnetization measurements of Fe_3Mo_3N and Co_3Mo_3N, we infer that the IEMT and the χ-T maximum behavior are correlated in these systems [17,22]. As the χ-T maximum behavior remains up to $x = 0.05$, we can expect the onset of the IEMT in the doped samples. Figure 3 shows the curve corresponding to the pulse high-field magnetization measurements at 4.2 K for several compositions. As expected, we observed IEMTs along with hysteresis in the composition range $0 \leqslant x \leqslant 0.04$.

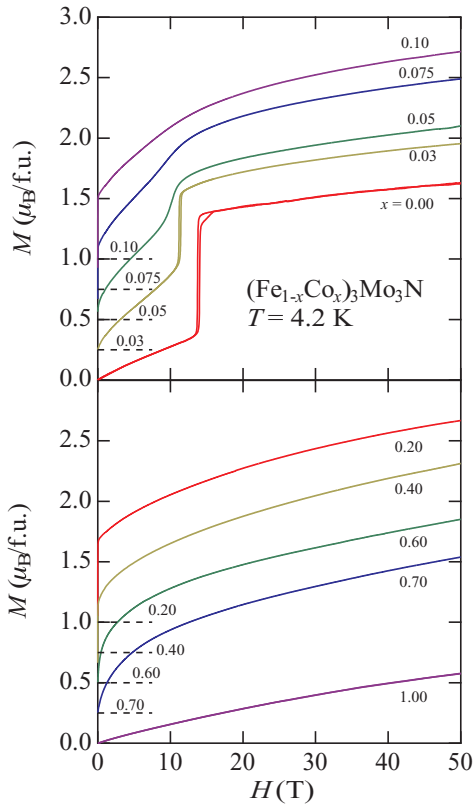

FIG. 3. (Color online) High-field magnetic isotherms measured at 4.2 K for selected samples with different compositions. Data are offset in increments of 0.25 μ_B/f.u. Dashed lines represent origins.

Interestingly, we observed the coexistence of doping-induced ferromagnetism and metamagnetic transitions for the range $0.05 \leqslant x \leqslant 0.10$. When $0.075 \leqslant x \leqslant 0.10$, low-temperature CW-type enhancement due to impurity or randomness may suppress the χ-T maximum. Above the transition, the magnetization increases without saturation, thereby showing an itinerant electron magnetic character. For $0.20 \leqslant x \leqslant 0.60$, the magnetization increases rapidly at very low fields and increases monotonically at high fields, suggesting the occurrence of itinerant ferromagnetism. For $x \geqslant 0.65$, no spontaneous moment exists at the lowest temperature although the magnetization curve is not linear. In some WIEFs, a metamagnetic transition was observed at the critical concentration at which T_C becomes zero. However, we did not observe any anomaly in the magnetization curve at $x \simeq 0.65$. For $x = 1.00$, the magnetization increases almost linearly.

Metamagnetism at $0 \leqslant x \leqslant 0.04$ is accompanied by hysteresis, which suggests that the transition is of first order. The magnetic isotherms for these concentrations were examined at several temperatures. As an example, we depict the dM/dH curve of $x = 0.03$ in Fig. 4. At $T = 4.2$ K, divergent behaviors in dM/dH were observed at 11.2 and 11.4 T in field increasing and decreasing processes, respectively, thereby indicating the presence of hysteresis in the magnetization. The critical transition field H_c and the hysteresis width ΔH are defined as the averaged value and the difference, respectively. Further, $H_c = 11.3$ T at $T = 4.2$ K is reduced compared with that of Fe_3Mo_3N. With increasing temperature, the field at which dM/dH reaches a maximum increases but the anomaly becomes unclear. Further, ΔH decreases to zero at $T = 27$ K.

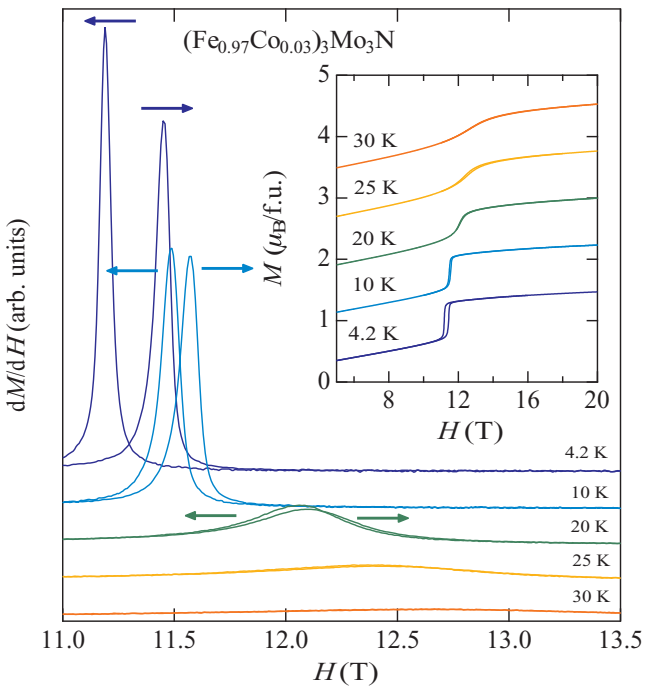

FIG. 4. (Color online) dM/dH curves for $x = 0.03$ at different temperatures. At $T = 4.2$ K, a sharp peak was observed both in field-increasing and decreasing processes with a hysteresis. The inset shows magnetic isotherms obtained by integrating dM/dH. The data are offset in increments of 0.8 μ_B/f.u.

TABLE II. CEP parameters H_{cr} and T_{cr} estimated from ΔH, and hypothetical spontaneous moment p_s^* estimated from the Arrott plot at 4.2 K.

x	H_{cr} (T)	T_{cr} (K)	p_s^* (μ_B/3d atom)
0.00	15.76	42	0.418
0.01	14.16	35	0.404
0.03	12.55	27	0.398
0.04	11.65	18	0.405

We determined the CEP temperature T_{cr} and the field H_{cr} to be 27 K and 12.5 T, respectively, as the temperature and the field at which ΔH becomes zero. The CEP for each composition is listed in Table II. Above this temperature, the anomaly in dM/dH was still observed, but the hysteresis disappears, thereby suggesting that the anomaly is actually a crossover. The crossover field also increases with increasing temperature. In Fe_3Mo_3N, another metamagnetic transition associated with a small jump was observed in the field-increasing process immediately after the large metamagnetic jump [17]. However, such an anomaly has not been observed in the doped compounds.

The metamagnetic transition for $0.05 \leqslant x \leqslant 0.10$ at $T = 4.2$ K is not associated with a hysteresis. To confirm the existence of a first-order transition below $T = 4.2$ K, we measured dM/dH at $T = 1.3$ K for the samples in which the alloying-induced ferromagnetism and the metamagnetic transition coexist (Fig. 5). For $x = 0.05$, a peak was observed in the dM/dH curve at $H = 10.5$ T, but no hysteresis was observed with the experimental resolution, thus suggesting that the metamagnetism is a crossover and H_c should be less than $T = 1.3$ K. With increasing x, the crossover field decreases and the anomaly finally disappears.

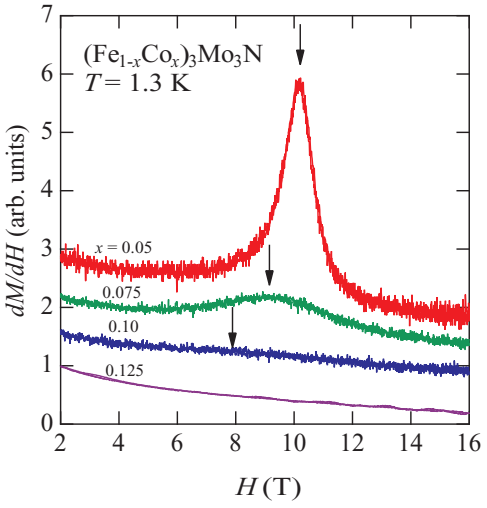

FIG. 5. (Color online) dM/dH for several compositions in which magnetization shows a rapid increase at low fields and an anomaly at finite fields. With increasing x, the anomaly in dM/dH is suppressed and the peak decreases to disappear at $x = 0.125$. Both the field-increasing and decreasing processes are shown. No hysteresis was observed in these compositions, suggesting that the anomalies were due not to a first-order transition but a crossover.

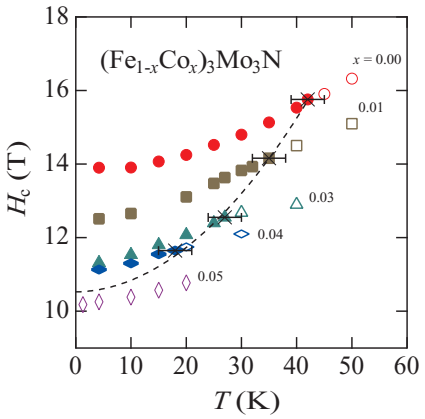

FIG. 6. (Color online) Temperature dependence of critical and crossover fields of IEMTs for different compositions. Solid and open markers represent the first-order transition and the crossover fields, respectively. The former was estimated as the average of the transition fields in field-increasing and field-decreasing processes. Crosses represent CEPs of the first-order transition that were estimated as the field and the temperature at which the hysteresis width $\Delta H \to 0$. The dashed line serves as a visual guide. The critical point shifts downward in terms of field and temperature with increasing x, and zero temperature is reached at $x \simeq 0.05$, thus suggesting the existence of a QCEP.

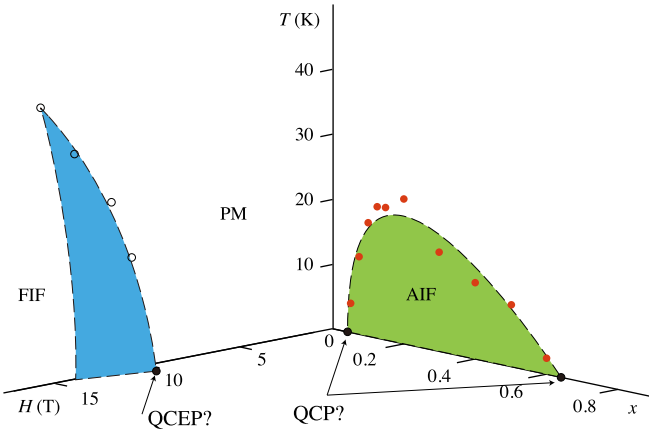

FIG. 7. (Color online) x-H-T phase diagram for $(Fe_{1-x}Co_x)_3Mo_3N$. Open and solid circles represent the CEP of the metamagnetic transition and T_C, respectively. Dashed lines are guide for the eyes.

Figure 6 shows the temperature dependence of the critical and the crossover fields for $0 \leqslant x \leqslant 0.05$. For $0 \leqslant x \leqslant 0.04$, H_c increases as T^2 and terminates at a certain point. This behavior is commonly observed in the materials which show IEMTs [23–25]. With increasing x, the CEP of this IEMT decreases rapidly in terms of the values of the temperature and field. Extrapolating the data from $x = 0$ to 0.04, we observed that the critical temperature reaches zero at a finite field value around $x = 0.05$, thereby suggesting the existence of the QCEP of this IEMT around $x = 0.05$ and $H_{cr} = 10.5$ T.

A sharp DOS immediately below the Fermi level is considered to be essential to exhibit the IEMT according to the band model [26,27]. The substitution effect on the YCo_2 system supports this picture; with increasing the number of electrons obtained by substituting Ni for Co, the Fermi level shifts upwards, resulting in an increase in the critical field that eventually splits the band, while the Fermi level shifts downwards to reduce the field in the Fe case [28]. On the contrary, the critical field of $(Fe_{1-x}Co_x)_3Mo_3N$ decreases with increasing electrons. A hole-type band immediately above the Fermi level may contribute to the IEMT in our case.

C. Phase diagram

The x-H-T phase diagram of $(Fe_{1-x}Co_x)_3Mo_3N$ is drawn in Fig. 7, where T_C and T_{cr} are transition temperatures for the AIF and the FIF, respectively. The AIF region with two QCPs appears in the range of $0.05 \leqslant x \leqslant 0.60$, where T_C reaches a maximum at $x = 0.20$. At $x \simeq 0.05$, the ferromagnetic transition is of first order like typical WIEFs, whereas at $x \simeq 0.60$ it is not the case. Interestingly, the AIF region is sandwiched by two paramagnetic metals, Fe_3Mo_3N and Co_3Mo_3N. In most pseudobinary magnetic phase diagrams, one of the end materials is magnetic but not the other. In Co-based C15 Laves-phase paramagnetic materials designated as RCo_2, where R = Sc, Y, and Lu, undergoing IEMTs at finite fields, ferromagnetism is induced by substituting nonmagnetic atoms for Co. However, any paramagnetic phases have not been observed in the highly doped regions due to the presence of the solubility limit [29–31].

For the FIF, the CEP of the IEMT starts from $(x, H, T) = (0,$ 15.76 T, 42 K) and decreases rapidly in terms of temperature and field with increasing x. Extrapolating the second-order critical line of the IEMT, the CEP reaches zero temperature at $(x, H) = (0.045,$ 10.5 T), thus suggesting the existence of a QCEP. The second-order critical line does not reach the AIF phase, indicating that the AIF and the FIF phases are separated in the x-H-T space. This is one of the most characteristic features of the obtained phase diagram.

IV. DISCUSSION

A. Separation of AIF and FIF

We obtained the magnetic phase diagram of $(Fe_{1-x}Co_x)_3Mo_3N$, in which the AIF and the FIF are separated in contrast to those of typical WIEFs. This kind of phase diagram cannot be reproduced by conventional theories for WIEFs.

Theoretical phase diagrams of WIEFs, including IEMTs, have been obtained in mainly two ways. One is the phenomenological Landau's theory which takes into consideration up to the M^6 term in the magnetic free-energy expansion [32,33]. The expansion coefficients, which are related to the band structure and spin fluctuation, are tuning parameters in obtaining the phase diagram [33]. The other is the mean-field theory based on microscopic excitations, which successfully explains low-temperature phase diagrams of WIEFs [8]. In both treatments, however, field-induced and zero-field ferromagnetic phases are merged in the phase diagrams. $(Fe_{1-x}Co_x)_3Mo_3N$ is not the case.

Probably the above theories are not applicable to our case because $(Fe_{1-x}Co_x)_3Mo_3N$ is not a simple WIEF for two reasons. First, there are two crystallographically inequivalent sites which are responsible for the magnetism (16*d* and 32*e* in $Fd\bar{3}m$), resulting in multiple bands. Second, associated with this fact, both ferromagnetic and antiferromagnetic interactions may compete in this system as neutron scattering experiment actually detected antiferromagnetic correlation in spite of the ferromagnetic NFL behavior [17]. Recently, it has been reported that partially Ge substituted Fe_2GeMo_3N exhibits Néel order at a fairly high temperature ($T_N = 455$ K) [34], despite the fact that the host Fe_3Mo_3N does not show any magnetic transition. In Fe_2GeMo_3N, Ge preferentially occupies the 16*d* site and Fe occupies the 32*e* site to form Fe tetrahedral clusters. The absence of 16*d* Fe releases the frustration in the pyrochlore lattice. It is speculated that each Fe sublattice possesses different spin fluctuation.

If the metamagnetic transition is caused by competitive spin fluctuations, the metamagnetic transition in this system is analogous to that of $CeRu_2Si_2$ [35,36] and $YbRh_2Si_2$ [37,38] in which reconfiguration of the Fermi surface occurs in magnetic field, rather than that of typical WIEFs described using a free energy with higher terms. According to Takahashi and Sakai, the IEMT is a phase transition between a paramagnetic state and a ferromagnetic state with different free energies, and the Arrott plot is expected to be linear for each phase [39]. The linearity of the Arrott plot for the FIF phase should be a good test for checking whether the FIF has a different Fermi surface from that of a paramagnetic state because single free energy which describes the IEMT does not give a linear relation of the Arrott plot at the FIF region.

Figure 8 shows Arrott plots at $T = 4.2$ K up to high fields for the samples which show IEMT. Similar to $Y(Co_{0.91}Al_{0.09})_2$ [39] and $LaCo_9S_4$ [40] cases, a reasonably good degree of linearity above the metamagnetic transition is observed, thus suggesting another type of IEMTs. The extrapolated value at M^2 at $H = 0$ yields the hypothetical spontaneous moment p_s^* of the FIF. The results are listed in Table II.

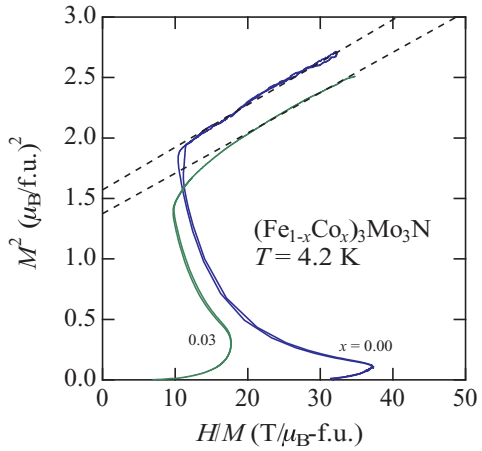

FIG. 8. (Color online) Arrott plots at high magnetic fields and at $T = 4.2$ K. Dashed lines indicate the best linear fit for field-induced phases.

B. Analysis using spin fluctuation theory

Itinerant electron magnetism is characterized by the spin fluctuation parameters T_A and T_0, which are measures of the spectral widths in the wave vector and energy spaces, respectively. The AIF and the FIF phases are separated in the obtained phase diagram, thus suggesting that these ferromagnetism should have different T_A and T_0. Here we estimate T_A and T_0 using macroscopic magnetization, while, in principle, they can directly be estimated by neutron scattering and NMR relaxation time measurements. In Takahashi's spin fluctuation theory, which takes into account the zero-point fluctuation and assumes the conservation of spin amplitude, these parameters can be estimated via macroscopic magnetic measurements for the WIEF [41–43]. The coexistence of ferromagnetic and antiferromagnetic correlations in Fe_3Mo_3N [17] may make it unreliable to apply the spin fluctuation theory for WIEFs to the $(Fe_{1-x}Co_x)_3Mo_3N$ system. However, since the system behaves as a WIEF at least macroscopically, we attempt to apply the theory.

At zero temperature, the assumption of the spin-amplitude conservation yields the following relation for the magnetization:

$$H = \frac{2T_A^2}{15cN_0^3(g\mu_B)^4T_0}\left(-M_0^2 + M^2\right)M, \tag{2}$$

where g represents Lande's g factor, $c = 1/2$, and M_0 denotes the spontaneous moment. By modifying this equation, the theoretical equation underlying the Arrott plot is obtained as follows:

$$H/M = a(0) + b(0)M^2, \tag{3}$$

$$a(0) = -\frac{M_0^2}{b(0)}, b(0) = \frac{F_1}{N_0^3(g\mu_B)^4}, \tag{4}$$

$$F_1 = \frac{2T_A^2}{15cT_0}. \tag{5}$$

F_1 is experimentally obtained from the slope of the Arrott plot at zero temperature ξ as

$$F_1 = N_0^3(2\mu_B)^4/\xi k_B. \tag{6}$$

When $T/T_0 \ll 1$, the following relations are also derived:

$$\left(\frac{T_C}{T_A}\right)^{5/3} = \frac{p_s^2}{5g^2C_{4/3}}\left(\frac{2T_C}{15cF_1}\right)^{1/3}, \tag{7}$$

$$\left(\frac{T_C}{T_0}\right)^{5/6} = \frac{p_s^2}{5g^2C_{4/3}}\left(\frac{15cF_1}{2T_C}\right)^{1/2}, \tag{8}$$

where $C_{4/3} = 1.00608\ldots$. We can estimate T_A and T_0 using these relations and the values of F_1, T_C, and p_s obtained by macroscopic magnetic measurements.

We can safely estimate F_1 for the FIF ($0 \leqslant x \leqslant 0.04$) and the AIF ($0.05 \leqslant x \leqslant 0.6$) from the values of ξ at 4.2 and 1.8 K, respectively, which can be regarded as sufficiently compared with the critical temperatures. The obtained values of F_1 are listed in Table III. F_1 is $\sim 8.5 \times 10^3$ K, and it is independent

TABLE III. (Color online) Spin fluctuation parameters F_1, T_0, and T_A deduced from magnetic measurement. The ratios $p_{\rm eff}/p_{\rm s}$ and $T_{\rm C}/T_0$ are also listed.

x	F_1 (K)	T_0 (K)	T_A (K)	$p_{\rm eff}/p_{\rm s}$	$T_{\rm C}/T_0$
0.00	8.29×10^3	237	2.71×10^3	5.22	0.177
0.01	9.03×10^3	183	2.49×10^3	5.82	0.191
0.03	8.74×10^3	128	2.04×10^3	5.46	0.212
0.04	8.32×10^3	66	1.43×10^3	5.16	0.274
0.05	2.01×10^4	727	7.40×10^3	48.5	0.00551
0.075	8.35×10^3	649	4.66×10^3	17.2	0.0173
0.10	4.67×10^3	657	3.39×10^3	12.3	0.0266
0.125	4.53×10^3	658	3.34×10^3	10.8	0.0308
0.15	3.97×10^3	576	2.93×10^3	9.98	0.0355
0.20	4.37×10^3	576	3.07×10^3	9.65	0.0387
0.30	4.39×10^3	489	2.84×10^3	11.1	0.0314
0.40	5.57×10^3	425	2.98×10^3	12.6	0.0277
0.50	5.62×10^3	363	2.77×10^3	13.4	0.0261
0.60	4.94×10^3	340	2.51×10^3	32.0	0.00735

of x in the range $0 \leqslant x \leqslant 0.04$. With increasing x, F_1 of the AIF rapidly decreases from 2.0×10^4 K at $x = 0.05$ to nearly x-independent values of 4–6 $\times 10^3$ K. Paramagnetic samples beyond $x = 0.60$ also exhibit $F_1 \simeq 6 \times 10^3$ K, thus suggesting the existence of an analogous electronic state in the concentration range.

Using these values, we obtained values of T_A and T_0 for both FIF and AIF [Figs. 9(a) and 9(b)]. For the analysis of the FIF, we treated $p_{\rm s}^*$ and $T_{\rm cr}$ as the saturation moment and the Curie temperature, respectively. In the FIF, T_A and T_0 rapidly decrease with increasing x. In the AIF ($x \geqslant 0.05$), T_0 decreases monotonically, while T_A decreases rapidly at first and tends to remain constant at $\sim 3 \times 10^3$ K. T_A and T_0 for the FIF and the AIF are discontinuous at $x = 0.05$, thus suggesting that the FIF and the AIF are characterized by different spin fluctuations.

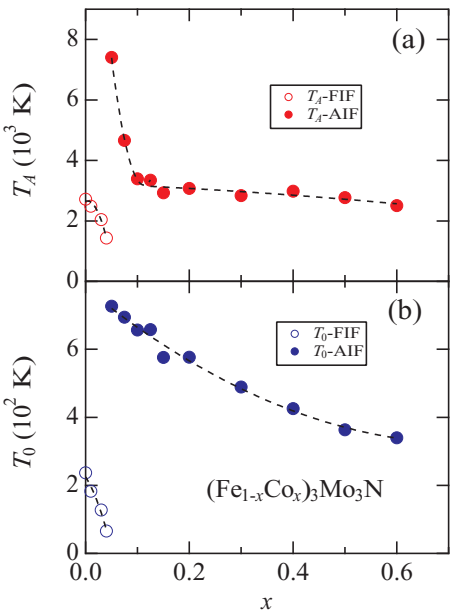

FIG. 9. (Color online) (a) T_A vs x. (b) T_0 vs x. Open and solid circles represent the data for FIF and AIF, respectively.

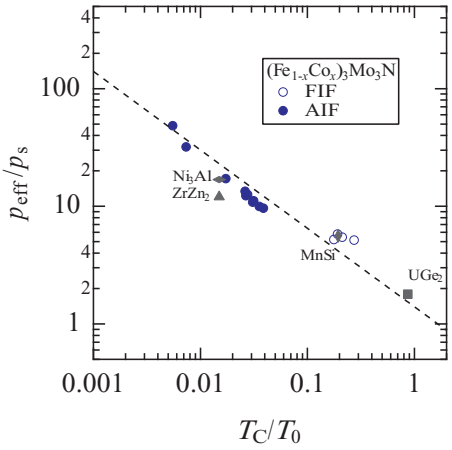

FIG. 10. (Color online) Takahashi-Rhodes-Wohlfarth plot or Deguchi-Takahashi plot for parameters of AIF and FIF. Data for $ZrZn_2$, Ni_3Al, MnSi, and UGe_2 are also plotted (Ref. [43]).

T_0 is an important parameter that characterizes the energy scale of a phase transition. For example, it is known that T_0 scales the superconducting critical temperature [44]. For the WIEF, the following Takahashi-Rhodes-Wohlfarth relation has been obtained:

$$\frac{p_{\rm eff}}{p_{\rm s}} \simeq 1.4 \left(\frac{T_{\rm C}}{T_0} \right)^{-2/3}. \tag{9}$$

Figure 10 shows the double logarithmic plot of $p_{\rm eff}/p_{\rm s}$ vs $T_{\rm C}/T_0$ for the FIF and the AIF. The corresponding data of typical WIEFs are also included. As regarded the values of $p_{\rm eff}$ for the FIF, we used the values obtained from the Curie susceptibility at low fields because it is practically impossible to estimate $p_{\rm eff}$ at high fields. However, this is not an unreasonable estimation considering the fact that the magnetic isotherm of Fe_3Mo_3N is linear up to high fields at $T = 100$ K (not shown). The data points of the AIF and the FIF are observed near the line, but they lie in two regions corresponding to large and small $T_{\rm C}/T_0$ values.

As seen above, the electronic states of the AIF and the FIF are expected to be different. It is valuable to evaluate spin fluctuation parameters for each phase in order to understand the phase diagram of WIEFs. The $Y(Co_{1-x}Al_x)_2$ system is a rare example for which the parameters have been determined by microscopic experiments; T_0s in the paramagnetic phase and of the AIF show divergent behaviors at around the paramagnetic-ferromagnetic phase boundary, although T_0 for the FIF has not been evaluated [45]. To reveal the spin fluctuation spectrum of our system using microscopic methods is a future issue.

V. SUMMARY

We performed comprehensive magnetization measurements on itinerant-electron magnetic nitrides $(Fe_{1-x}Co_x)_3Mo_3N$. We observed a ferromagnetic phase with the transition temperature up to 22.3 K in the composition range $0.05 \leqslant x \leqslant 0.60$ and a field-induced first-order

ferromagnetic transition in $0.00 \leqslant x \leqslant 0.04$. The AIF and the FIF phases are separated in the constructed x-H-T magnetic phase diagram, which is different from those of conventional WIEFs. There are two QCPs for the ferromagnetism at $x \simeq 0.05$ and 0.60, and one QCEP corresponding to the IEMT at $x = 0.05$ and $H_{cr} = 10.5$ T. An analysis using the spin fluctuation theory reveals that the spin fluctuation spectra in the AIF and the FIF are different from each other, supporting that the IEMT in this system is associated with reconfiguration of the electric state.

ACKNOWLEDGMENTS

We thank K. Yoshimura and Y. Takahashi for discussion. This study was supported by a Grant-in-Aid for Scientific Research on Priority Areas "Novel States of Matter Induced by Frustration," a Grant-in-Aid for the Global COE Program, "International Center for Integrated Research and Advanced Education in Materials Science," and a Grant-in-Aid for Young Scientists (B) 21760531 from the Ministry of Education, Culture, Sports, Science and Technology of Japan.

[1] T. Moriya, *Spin Fluctuations in Itinerant Electron Magnetism* (Springer, Berlin Heidelberg, 1985).
[2] Q. Si and F. Steglich, Science **329**, 1161 (2010).
[3] T. Shibauchi, A. Carrington, and Y. Matsuda, Annu. Rev. Condens. Matter Phys. **5**, 113 (2014).
[4] C. Pfleiderer and A. D. Huxley, Phys. Rev. Lett. **89**, 147005 (2002).
[5] C. Pfleiderer, G. J. McMullan, S. R. Julian, and G. G. Lonzarich, Phys. Rev. B **55**, 8330 (1997).
[6] M. Uhlarz, C. Pfleiderer, and S. M. Hayden, Phys. Rev. Lett. **93**, 256404 (2004).
[7] M. Nicklas, M. Brando, G. Knebel, F. Mayr, W. Trinkl, and A. Loidl, Phys. Rev. Lett. **82**, 4268 (1999).
[8] D. Belitz, T. R. Kirkpatrick, and J. Rollbühler, Phys. Rev. Lett. **94**, 247205 (2005).
[9] V. Taufour, D. Aoki, G. Knebel, and J. Flouquet, Phys. Rev. Lett. **105**, 217201 (2010).
[10] S. A. Grigera, R. S. Perry, A. J. Schofield, M. Chiao, S. R. Julian, G. G. Lonzarich, S. I. Ikeda, Y. Maeno, A. J. Millis, and A. P. Mackenzie, Science **294**, 329 (2001).
[11] H. Kotegawa, V. Taufour, D. Aoki, G. Knebel, and J. Flouquet, J. Phys. Soc. Jpn. **80**, 083703 (2011).
[12] D. Aoki, T. Combier, V. Taufour, T. D. Matsuda, G. Knebel, H. Kotegawa, and J. Flouquet, J. Phys. Soc. Jpn. **80**, 094711 (2011).
[13] J. A. Hertz, Phys. Rev. B **14**, 1165 (1976).
[14] A. J. Millis, Phys. Rev. B **48**, 7183 (1993).
[15] T. Waki, S. Terazawa, Y. Tabata, F. Oba, C. Michioka, K. Yoshimura, S. Ikeda, H. Kobayashi, K. Ohoyama, and H. Nakamura, J. Phys. Soc. Jpn. **79**, 043701 (2010).
[16] T. J. Prior and P. D. Battle, J. Mater. Chem. **14**, 3001 (2004).
[17] T. Waki, S. Terazawa, T. Yamazaki, Y. Tabata, K. Sato, A. Kondo, K. Kindo, M. Yokoyama, Y. Takahashi, and H. Nakamura, Europhys. Lett. **94**, 37004 (2011).
[18] T. Goto, K. Fukamichi, and H. Yamada, Physica B **300**, 167 (2001).
[19] M. Ohta, K. Fukamichi, A. Fujita, H. Saito, and T. Goto, J. Alloys Compd. **394**, 43 (2005).
[20] K. Fukamichi, *Handbook of Advanced Magnetic Materials*, (Springer, New York, 2006), Vol. 2, Chap. 7.
[21] T. J. Prior and P. D. Battle, J. Solid State Chem. **172**, 130 (2003).
[22] T. Waki, Y. Umemoto, S. Terazawa, Y. Tabata, A. Kondo, K. Sato, K. Kindo, S. Alconchel, F. Sapiña, and H. Nakamura, J. Phys. Soc. Jpn. **79**, 093703 (2010).
[23] K. Murata, K. Fukamichi, T. Sakakibara, T. Goto, and H. Aruga-Katori, J. Phys.: Condens. Matter **5**, 2583 (1993).
[24] T. Goto, Y. Shindo, H. Takahashi, and S. Ogawa, Phys. Rev. B **56**, 14019 (1997).
[25] K. Fukamichi, T. Yokoyama, H. Saito, T. Goto, and H. Yamada, Phys. Rev. B **64**, 134401 (2001).
[26] M. Cyrot and M. Lavagna, J. Appl. Phys. **50**, 2333 (1979).
[27] H. Yamada, J. Inoue, K. Terao, S. Kanda, and M. Shimizu, J. Phys. F: Met. Phys. **14**, 1943 (1984).
[28] T. Sakakibara, H. Mitamura, and T. Goto, Physica B **201**, 127 (1994).
[29] K. Ishiyama and K. Endo, J. Phys. Soc. Jpn. **55**, 2535 (1986).
[30] K. Yoshimura and Y. Nakamura, Solid State Commun. **56**, 767 (1985).
[31] K. Endo, M. Iijima, A. Shinogi, and K. Ishiyama, J. Phys. Soc. Jpn. **56**, 1316 (1987).
[32] M. Shimizu, J. Physique **43**, 155 (1982).
[33] H. Yamada, Phys. Rev. B **47**, 11211 (1993).
[34] P. D. Battle, L. A. Sviridov, R. J. Woolley, F. Grandjean, G. J. Long, C. R. A. Catlow, A. A. Sokol, A. Walsh, and S. M. Woodley, J. Mater. Chem. **22**, 15606 (2012).
[35] H. Pfau, R. Daou, M. Brando, and F. Steglich, Phys. Rev. B **85**, 035127 (2012).
[36] A. Pourret, D. Aoki, M. Boukahil, J.-P. Brison, W. Knafo, G. Knebel, S. Raymond, M. Taupin, Y. Ōnuki, and J. Flouquet, J. Phys. Soc. Jpn. **83**, 061002 (2014).
[37] H. Pfau, R. Daou, S. Lausberg, H. R. Naren, M. Brando, S. Friedemann, S. Wirth, T. Westerkamp, U. Stockert, P. Gegenwart, C. Krellner, C. Geibel, G. Zwicknagl, and F. Steglich, Phys. Rev. Lett. **110**, 256403 (2013).
[38] A. Pourret, G. Knebel, T. D. Matsuda, G. Lapertot, and J. Flouquet, J. Phys. Soc. Jpn. **82**, 053704 (2013).
[39] Y. Takahashi and T. Sakai, J. Phys.: Condens. Matter **7**, 6279 (1995).
[40] H. Michor, M. El-Hagary, M. D. Mea, M. W. Pieper, M. Reissner, G. Hilscher, S. Khmelevskyi, P. Mohn, G. Schneider, G. Giester, and P. Rogl, Phys. Rev. B **69**, 081404 (2004).
[41] Y. Takahashi, J. Phys. Soc. Jpn. **55**, 3553 (1986).
[42] Y. Takahashi, J. Phys.: Condens. Matter **13**, 6323 (2001).
[43] Y. Takahashi, *Spin Fluctuation Theory of Itinerant Electron Magnetism* (Springer, Berlin Heidelberg, 2013).
[44] T. Moriya and K. Ueda, Rep. Prog. Phys. **66**, 1299 (2003).
[45] K. Yoshimura, M. Mekata, M. Takigawa, Y. Takahashi, and H.Yasuoka, Phys. Rev. B **37**, 3593 (1988).